

# Spectral imaging of skin: experimental observations and analyses

John Kerekes<sup>a\*</sup>, Nithya Subramanian<sup>b</sup>, Kevin Kearney<sup>c</sup>, Nik Schad<sup>c</sup>

<sup>a</sup>Center for Imaging Science, Rochester Inst. of Tech, 54 Lomb Memorial Dr, Rochester, NY 14623

<sup>b</sup>Dept. of Electrical Eng., Rochester Inst. of Tech, 79 Lomb Memorial Dr, Rochester, NY 14623

<sup>c</sup>Geospatial Systems, Inc., 125 Tech Park Dr., Rochester, NY 14623

## ABSTRACT

The emergence of compact optical spectral imaging technologies has motivated the study of their use in a variety of applications, including medical diagnosis and monitoring. In particular, large format CCD focal planes in conjunction with spectrally tunable devices offer enhanced spatial information together with visible and near infrared (NIR) spectroscopic data for the passive, noninvasive, measurement of human skin and near surface tissue characteristics. One such spectral imaging system was recently developed by mating a Liquid Crystal Tunable Filter (LCTF) together with a 2048x2048 silicon CCD focal plane. This system is capable of collecting more than 30 co-registered spectral images spaced every 10 nanometers and spanning 400 to 720 nanometers. This system combines the potential of near infrared diffuse reflectance spectroscopy with the high spatial resolution of traditional optical imaging techniques. Spectral images were acquired of portions of the hands and arms of several test subjects with a variety of features observable. The observations were collected in a “light box” under controlled illumination conditions. Images of a diffuse reflectance standard and instrument dark frames were collected to allow conversion of the raw images to spectral reflectance images. This paper presents examples of the spectral images collected, instrument characteristics and performance, and results of analysis algorithms applied to the data. Results also are shown for a new algorithm extracting the saturated oxygen hemoglobin fraction from these data.

Keywords: Novel optical techniques, spectral imaging

## 1. INTRODUCTION

The emergence of compact optical spectral imaging technologies has motivated the study of their use in a variety of applications, including medical diagnosis and monitoring. In particular, large format CCD focal planes in conjunction with spectrally tunable devices offer enhanced spatial information together with visible and near infrared (NIR) spectroscopic data for the passive, noninvasive, measurement of human skin and near surface tissue characteristics. These types of data have been demonstrated to have utility for the retrieval of hemoglobin characteristics<sup>1</sup> and the classification of skin lesions<sup>2</sup> among other applications.

One such spectral imaging system was recently developed at Geospatial Systems, Inc.<sup>3</sup> (GSI) by mating a Liquid Crystal Tunable Filter (LCTF) together with a 2048x2048 silicon CCD focal plane. This system is capable of collecting more than 30 co-registered spectral images spaced every 10 nanometers and spanning 400 to 720 nanometers. It combines the potential of near infrared diffuse reflectance spectroscopy with the high spatial resolution of traditional optical imaging techniques.

To begin investigating the potential medical applications of such an instrument, spectral images were acquired of portions of the hands and arms of several test subjects. The observations were collected in a “light box” under controlled illumination conditions. Images of a diffuse reflectance standard and instrument dark frames were collected to allow conversion of the raw images to spectral reflectance images. This paper presents examples of the spectral images collected, instrument characteristics and performance, and results of analysis algorithms applied to the data. Results also are shown for a new algorithm extracting the saturated oxygen hemoglobin fraction from these data.

---

\* kerekes@cis.rit.edu.

## 2. EXPERIMENTAL DATA COLLECTION

### 2.1 Instrument description

The V700 Imaging Spectrometer under development at GSI consists of three main components mated together with control electronics and software. The imaging sensor consists of a low noise 2048x2048 pixel digital camera manufactured by Redlake, LLC. The spectral measurements are made through the use of a LCTF manufactured by Cambridge Research Instrumentation, Inc. This device filters light in a narrow spectral bandpass (~10 nm) centered on a wavelength selected under software control. The spectrum for each pixel is measured by stepping through sequential wavelengths over time. A custom optical system mates the entrance aperture to the LCTF and the camera. Figure 1 shows the system at the prototype stage.

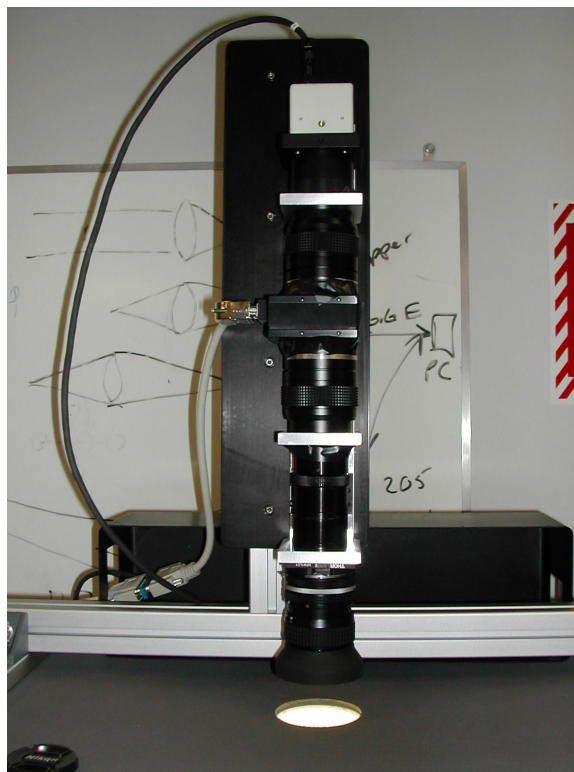


Figure 1. Prototype of the V700 Imaging Spectrometer.

The data collected by the instrument is written to disk in a format compatible with the analysis package ENVI<sup>4</sup> developed by Research Systems, Inc. The use of a commercial off the shelf analysis package reduced development costs and allowed us to take advantage of the extensive suite of existing spectral imagery analysis algorithms.

### 2.2 Data collection configuration

The imaging spectrometer was mounted above a light box looking through an entrance aperture at the top of the box. Inside the box, an array of high-intensity light bulbs was arranged to illuminate the test subject. The imaging spectrometer was configured with a standard 35 mm lens set at f/8. Given the distance between the camera and the test subject, the pixels on the subject's skin were approximately 0.13 mm. Thus the full 2048x2048 frame imaged an area approximately 10"x10". Figure 2 shows the configuration as used with our test subjects. As can be seen, the subject placed their hand and forearm in the field of view of the imaging spectrometer keeping them motionless for the duration of the data collection. A variable integration time was used for each of the bands ranging from a few tenths of a second to three seconds for the wavelengths where the LCTF has low light transmittance. Overall, it took about one minute to collect the full hypercube.



Figure 2. Experimental set-up with the imaging spectrometer, light box, and test subject.

### 2.3 Data pre-processing

In order to normalize out effects of the illumination and camera non uniformity, two additional measurements were made in conjunction with the test subject measurements. First, a cover was placed over the imaging spectrometer's lens, and a dark frame collected to provide a zero reference. Second, a panel of a diffuse reflectance standard, Spectralon™, was placed in the light box and a measurement made to capture the illumination field. Then the test subject placed their hand in the box and the test measurement made.

For each pixel  $i,j$ , and each wavelength  $\lambda$ , the diffuse reflectance  $\rho(i,j,\lambda)$  was then calculated by the following equation.

$$\rho(i,j,\lambda) = \frac{t(i,j,\lambda) - d(i,j,\lambda)}{s(i,j,\lambda) - d(i,j,\lambda)} \quad (1)$$

Here  $t()$  is the measurement of the test subject,  $d()$  is the measurement of the dark frame, and  $s()$  is the measurement of the Spectralon™ sample. Figure 3 shows some example raw measurements and the corresponding diffuse reflectance measurement for a sample area of skin.

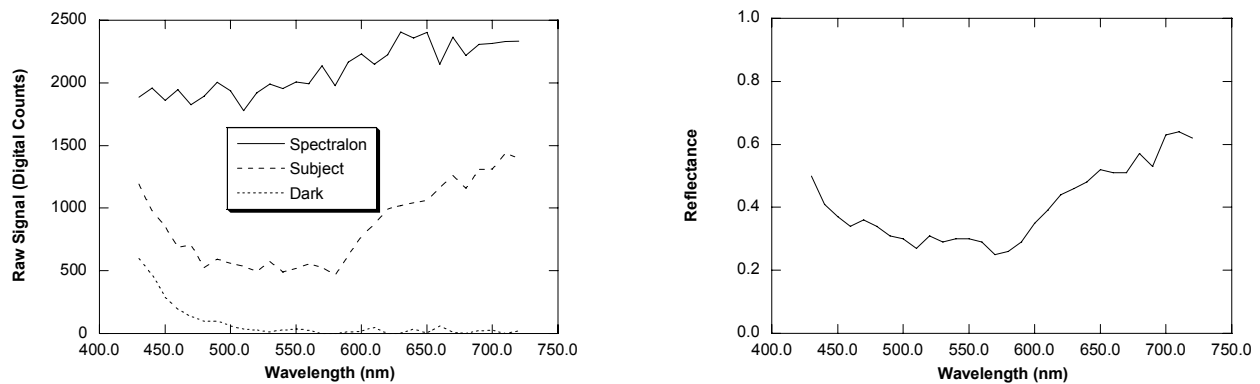


Figure 3. Example raw signals (left) and resulting reflectance (right) for a given pixel from an area of a test subject's palm.

### 3. EXPERIMENTAL OBSERVATIONS

Spectral hypercubes were collected for six volunteer test subjects as well as the Spectralon™ reflectance standard and the dark frames used for the conversion to reflectance. Figure 4 shows a portion of one of the test subject hypercubes including the subject's palm and base of thumb. The face of the cube is rendered in natural color using three bands of the cube and displaying on the monitor as RGB. That is, the image in band 24 (660 nm) is displayed on the red channel, band 13 (550 nm) is displayed on the green channel, and band 6 (480 nm) is displayed on the blue channel. The rainbow pseudo-coloring at the edges shows the spectrum of the edge pixels and graphically illustrates the concept of the hypercube with a full spectrum measured for every pixel in the image. Figure 5 shows another image and the corresponding reflectance spectra for the various points indicated on the image.

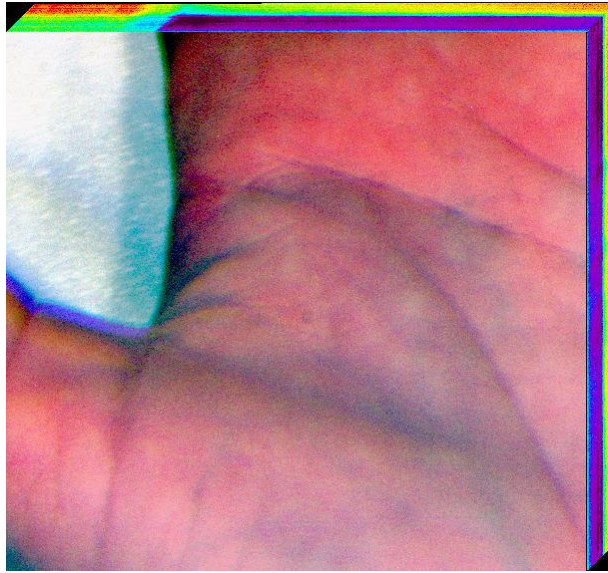


Figure 4. Example portion of a spectral image cube showing the concept of a spectrum “behind” every pixel.

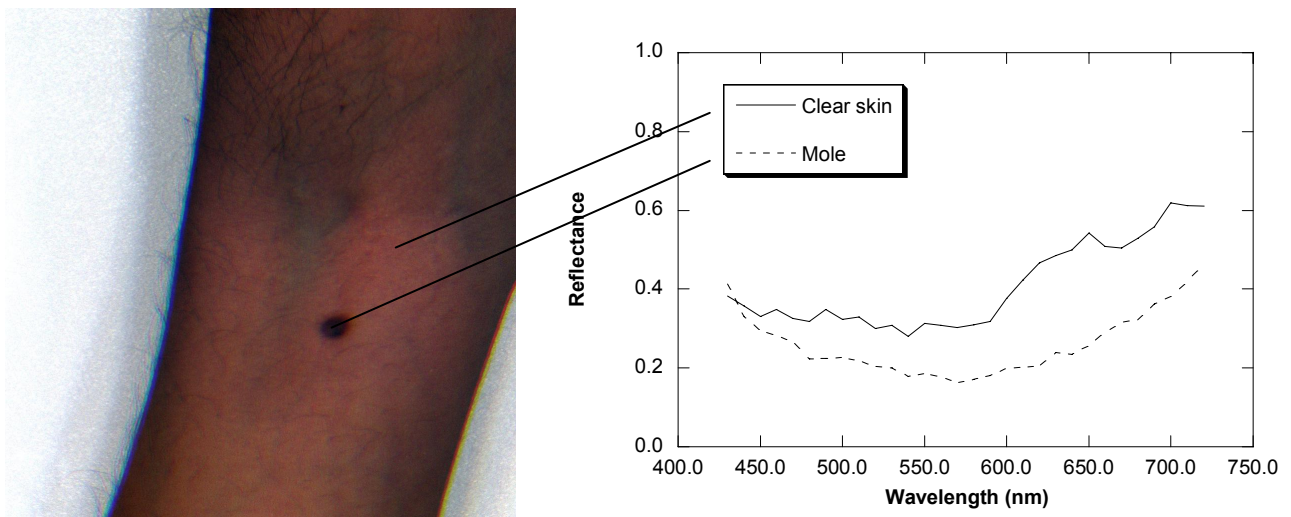
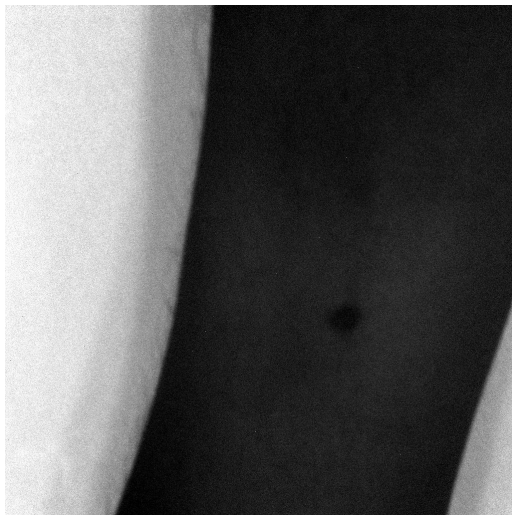


Figure 5. Natural color RGB image (left) and resulting measured spectral reflectance (right) for an area of clear skin and a mole.

It is interesting to observe how the skin appears at the across the different wavelengths collected. Figure 6 shows single band images from a sample of the range of wavelengths measured by the imaging spectrometer. A few observations can be noted. One, the images of the skin areas do become brighter as we move from the blue portion of the spectrum (450 nm) to the infrared (720 nm). This is consistent with the higher reflectance observed at the longer wavelengths as shown in the right side of Figure 5. Also, the skin becomes more transparent at these longer wavelengths as is evidenced by stronger contrast of the blood vessels as they appear. These observations are consistent with well known characteristics of skin.



a) 450 nm



b) 540 nm



c) 630 nm



d) 720 nm

Figure 6. Single band images from the wavelengths indicated.

#### 4. INSTRUMENT CHARACTERISTICS

Two instrument characteristics were studied with the data collected. The radiometric performance (noise level) was evaluated using the hypercubes of the Spectralon™ and the dark frame. A 500 x 500 pixel region was selected in the middle of the Spectralon™ image to reduce effects from variation in illumination over the scene. For each of the spectral bands, the mean and standard deviation of the raw pixel counts were calculated and the signal-to-noise ratio (SNR) computed as the ratio of the mean to the standard deviation. The same procedure was applied to the dark frame. Figure 7 below shows the resulting SNR estimated for these two cases.

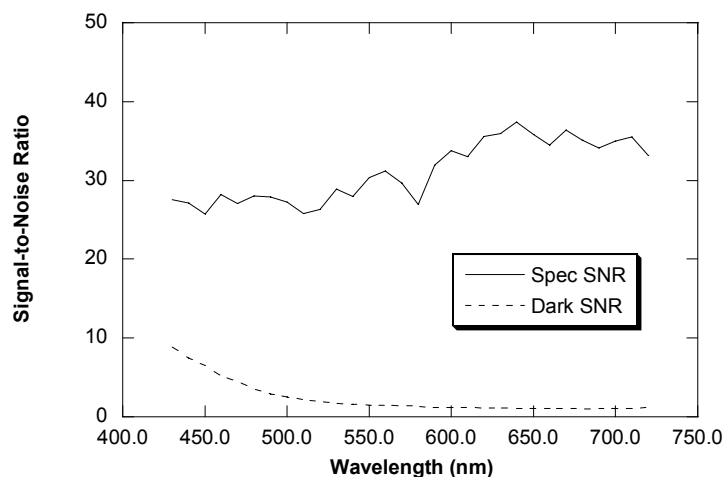


Figure 7. Empirical estimates of the SNR for Spectralon (solid) and dark frame (dashed).

The estimated SNR for the Spectralon™ is fairly constant in the 30-35 range. The variation across wavelength is most likely dominated by variations in the signal measured caused by non-uniform integration times across the bands. The SNR reported for the dark frame shows the readout electronics noise was on the order of the dark counts in the detector for most of the wavelength range.

The other instrument characteristic investigated was the spectral registration. This refers to the potential spatial offsets between images corresponding to different bands. To determine this offset, the image of the Spectralon™ plate was used. Since the plate was smaller than the instrument field of view, corners of the plate were visible and offered an easily identifiable location to track across the bands. The pixel location in the band 1 image corresponding to one corner of the plate was noted. Each band was then displayed and the pixel location noted for that corner. The difference between these locations thus determined the offset. Figure 8 plots the row and column offset thus determined.

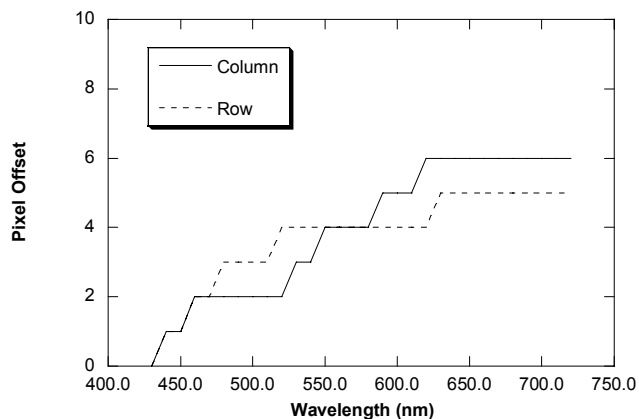


Figure 8. Estimates of the image misregistration between band 1 (430 nm) and each subsequent band.

A reason for this spectral misregistration could be the combination of a slight misalignment in the optics, together with uncompensated chromatic aberration. While this artifact will be minimized as the development moves from prototype to production, one way to minimize its effect is spatially filter the image resulting in reduced resolution. That is, by aggregating 5 x 5 pixel regions into a single pixel, the effects of the misregistration would be reduced. Since the original pixels were approximately 0.13 mm, these new pixels would still be less than 1 mm, providing sufficient spatial resolution for analysis.

## 5. PROCESSING RESULTS

One application for the spectral imaging data that we have been exploring is the retrieval of the spatial distribution of the fraction of oxygenated hemoglobin in the near surface tissue. A companion paper<sup>5</sup> describes the full procedure, but Figure 9 is included below to show an example of the results. In particular, these results demonstrate that the raw data has sufficient noise present to make the oxygen saturated fraction algorithm retrieve unreasonable results (Figure 9b). However, after performing a principal components transformation, keeping only the components associated with eigenvalues summing to 99% of the total, and then inverse transforming to the original domain (the process is referred to as Principal Component Analysis or PCA in the figure), the results of the algorithm are much more reasonable providing the range shown in Figure 9c.

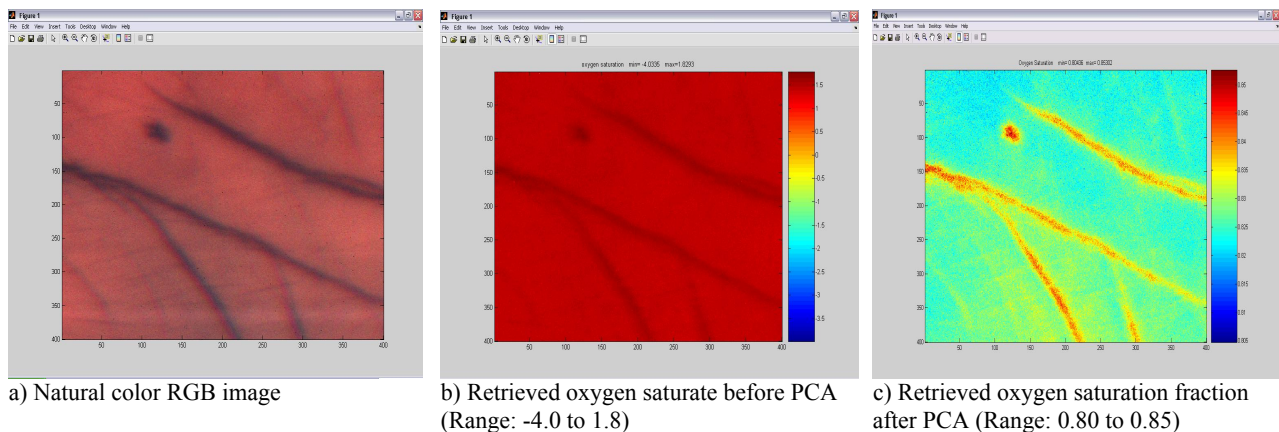


Figure 9. Example analysis results for the retrieval of the oxygen saturation fraction.

## 6. SUMMARY AND FUTURE WORK

Results have been presented from an experiment using an imaging spectrometer to collect spectral hypercubes of human skin. The instrument and data collection configuration were described and example imagery presented. The SNR and spectral registration errors of the instrument were characterized from the data collected. Finally, results of an algorithm retrieving the fraction of oxygenated hemoglobin were shown.

The results shown demonstrate the potential use of such imaging spectrometers for the distributed spatial measurement of near-surface skin characteristics such as the oxygen saturation fraction. These measurements (and others not shown in the paper) demonstrate significant spatial variability of the saturation fraction which may be helpful in diagnosis and localization for treatment. Through the collection of both spatial and spectral information simultaneously it is anticipated the combination will be much more helpful than just color images or single sample diffuse reflectance spectrometry measurements.

This experiment was an initial attempt to collect data and explore the potential applications. Since the time of data collection, the prototype instrument has been improved with lower noise and improved ease-of-use. In the future we hope to conduct more experiments to explore additional medical applications of spectral skin imaging.

## ACKNOWLEDGMENT

The authors acknowledge the support of this project by the Medical Science and Technology Center of the Eastman Kodak Company.

## REFERENCES

1. P. Dwyer, C. DiMarzio. "Hyperspectral imaging for dermal hemoglobin spectroscopy," SPIE Vol. 3752, pp 72-82, 1999.
2. M. Mehrubeoglu, N. Kehtarnavaz, G. Marquez, M. Duvic, and L.V. Wang. "Skin lesion classification using oblique-incidence diffuse reflectance spectroscopic imaging," *Applied Optics* Vol. 41, No. 1, pp.182-192, 2002.
3. [www.geospatialsystems.com](http://www.geospatialsystems.com).
4. [www.rsinc.com](http://www.rsinc.com)
5. N. Subramanian, J. Kerekes, K. Kearney, N. Schad, "Spectral imaging of near-surface oxygen saturation," *Proceedings of Physics of Medical Imaging*, SPIE Vol. 6142, to be published, 2006.